*Physicochem. Probl. Miner. Process., 55(1), 2019, 163-172*

http://www.journalssystem.com/ppmp

Physicochemical Problems of Mineral Processing

ISSN 1643-1049


*Received January 3, 2018; reviewed; accepted April 23, 2018*

# Fully coupled multi-physics modeling of the multi-type magnetic particles dynamic behavior in low intensity magnetic separator

**Feiwang Wang [1], Hongming Zhao [2], Huixin Dai [1], Wuxing Du [1]**

[1] Faculty of Land Resource Engineering, Kunming University of Science and Technology, Kunming, 650093, Yunnan, China
[2] State Key Laboratory of Complex Nonferrous Metal Resources Clean Utilization, Kunming, 50093, Yunnan, China

Corresponding author: dhx6688@sina.com (Huixin Dai)

**Abstract:** Studying the dynamic behavior of magnetic particle suspensions in the low intensity magnetic separator has important implications for various mineral beneficiation processes. A new approach for fully coupled multi-physics modeling of the dynamic behavior of multi-type magnetic particles (MTMPs) is developed in the study. In this model, the particle tracing module is employed to identify and determine individual particle trajectories in the fluid and magnetic field, which are modelled through the COMSOL Multiphysics. The results show that the different arrangements of the permanent magnet assembly and the volume percentage of interlocked particles affect the dynamic behavior of MTMPs and the efficiency of the separation. The model is compared with experiments and the particle capture theory and the correctness of the solution obtained from COMSOL is demonstrated. The model gives new possibilities to control, optimise, and develop the process of LIMS.

***Keywords:*** multi-physics model, low-intensity magnetic separator, magnetic particle, dynamic behavior

## 1. Introduction

In the mining industry, ferromagnetic particles (e.g. magnetite) are concentrated using wet low-intensity magnetic separation (LIMS) (Prakash et al., 2000; Kleiv et al., 2011; Tripathy et al., 2017). Ideally, all particles are liberated, all ferromagnetic particles together with a small portion of the water end up in the concentrate and all non-magnetic particles together with most of the water end up in the tailings product (Stener et al., 2016). However, the ore always contains unliberated material. When magnetite concentrate is upgraded to 67-68% Fe, $SiO_2$ grade in the concentrate is still high (3-7%), which causes a high energy consumption in smelting. It has been accepted that the reason is attributed to the entrainment of the locked quartz-magnetite particles into magnetite coagulates closely correlated with magnetic field intensity (Garcia-Martinez et al., 2011). However, in many situations the ferromagnetic particles transport inside a separator during various operating conditions is not sufficiently investigated. Wet LIMS begins to exhibit limitations when pushed to higher capacities and concentrate quality demands (Bikbov et al., 2004). The dynamic behavior of ferromagnetic particles in suspension is of interest for various mineral beneficiation processes. Although some experimentally motivated mathematical models such as Rayner (1999), Singh (2013), and Ersayin et al. (2013) exist in literature for LIMS, their application remains restricted to the estimation of mineral recovery as a function of various process parameters, without the ability to predict performance changes as a function of operating/design parameters of the separator. A typical LIMS involves multiple interacting physical phenomena, among which magnetism, fluid dynamics, particle kinetics and multibody contact are the dominant ones. Therefore, computational modelling approaches in a coupled-field framework are increasingly being adopted for the detailed analysis of LIMS.

One attempt at modelling the internal flow in a wet LIMS was made by Lejon Isaksson (2008), where a two-dimensional (2D) computational fluid dynamics (CFD) model of a wet LIMS was built. The boundary element method (BEM) for CFD analysis coupled with an analytically obtained magnetic field

DOI: 10.5277/ppmp18117

and a Lagrangian particle tracking approach, as shown in Ravnik and Hriberšek (2013), offers a computationally less expensive approach for modelling magnetic separation processes. However, its application is restricted to turbulent fluid flow problems with simple geometries. In Murariu et al. (2013), the discrete element method (DEM) is employed to identify and determine individual particle trajectories in a fluid and a magnetic field, which are modelled through CFD and finite element method (FEM), respectively. A similar framework was also employed for modelling a high gradient magnetic separator (HGMS) in Lindner et al. (2013). However, this model lacks a fully coupling model to calculate multiple interacting physical phenomena of the separation process using one FEM software at the same time. Another CFD approach assumes that the viscosity of the fluid (slurry) comprises water and magnetic particles and is a function of the magnetic particle concentration (Choomphon-Anomakhun et al., 2017). Although it enables the simulation of fairly large systems and allows a relatively accurate description of the slurry behavior that is captured and accumulated due to the attraction of the magnetic field, this method cannot consider the dynamic behavior at the multi-type magnetic particle level. Rasool (2018) presented a numerical modelling approach for wet high intensity magnetic separation (HIMS). The electromagnetic and the fluid flow field are modelled with the FEM, while the material particles are identified and evolved using the Level-set approach. However, this method is restricted to a very limited number of particles due to high computational expense and only binary systems where completely magnetic or non-magnetic particles are considered.

In this article, a novel and straightforward fully coupled multi-physics model is presented to investigate the 2D dynamic behavior of multi-type magnetic particles (MTMPs) in wet LIMS. In this model, the flow and magnetic fields are calculated by COMSOL Multiphysics version 5.2a at each simulation step. The particle tracing for fluid flow module is used to calculate the location and the dynamic behavior of MTMPs under the magnetic and flow fields. The effect of different permanent magnet assembly and the volume percentage of magnetite on separation efficiency and selectivity is investigated based on this model. The model gives new possibilities to control, optimise, and develop the process of LIMS.

## 2. Model description

LIMS has three different types, namely, concurrent (CC), counter-current (CTC), and counter-rotation (CR), depending on the slurry flow relative to the rotation of the drum. A wet LIMS consists of three main parts, namely, a rotating drum, a static permanent magnet assembly, and a tank (Stener et al., 2014). The non-magnetic cylindrical drum, typically made of stainless steel with rubber lining, contains a number of fixed magnets. The drum is partially submerged in a tank into which the ore pulp is fed. The magnetic particle is pulled toward the drum surface, carried across the magnetic poles, and removed from the tank. For a more detailed description see e.g. Sundberg (1998), Rayner and Napier-Munn (2000, 2003a, 2003b), and Stener (2016).

The FEM model described in this paper is developed for CR-type LIMS (Fig. 1) but can be easily adapted to any other types LIMS. These two different arrangements of magnetic poles close to the drum surface are the concurrent magnetic poles (CMP) and the alternating magnetic poles (AMP), established in COMSOL Multiphysics 5.2a, where all the ensuing model equations are set up and solved.

## 3. Basic principles

### 3.1. Modeling of slurry dynamic fluid behavior in tank

Fluid carries MTMPs into the magnetic field generated by a permanent magnet assembly. This slurry flows within a tank with different designs, depending on the configuration selected for the separation (Fig. 1). The flow of the slurry within the tank should be modeled to calculate the drag force that acts on the MTMPs. Reynolds number $Re$ is the most important non-dimensional number in Navier–Stokes dynamics. It describes the relative importance of inertial versus viscous effects as:

$$Re = \frac{\rho_w L \mathbf{u}}{\mu_w}, \tag{1}$$

where $\rho_w$ is the water density, $\mathbf{u}$ is the water velocity, $\mu_w$ is the water viscosity, and $L$ is the width of the separation area channel (Wilcox et al., 2006; Driver.,1985).

In the separation process, 997.1 kg · dm$^{-3}$ of water generally enters a 40 mm channel at 1 m · s$^{-1}$ velocity with 4481 Reynolds number. Thus, the fluid flow is always in the turbulent flow regime. The velocity of the fluid is described by the stationary Navier-Stokes and stationary continuity equations for uncompressible fluid flow.

$$\rho(\boldsymbol{u}\cdot\nabla)\boldsymbol{u} = \nabla\cdot[-p\boldsymbol{I} + \mu(\nabla\boldsymbol{u} + (\nabla\boldsymbol{u})^T)] + \boldsymbol{F} \tag{2}$$

$$\rho\nabla\cdot(\boldsymbol{u}) = 0, \tag{3}$$

where $p$ is the pressure, and **F** is the body force.

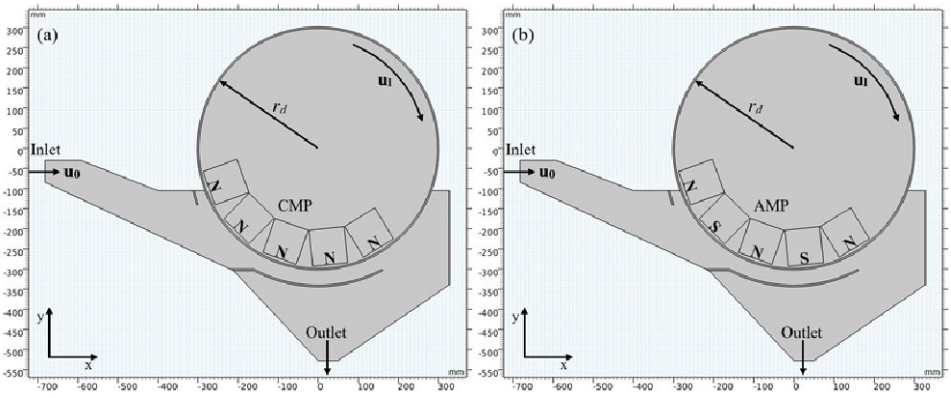


Fig. 1. Schematics of the 2-D CR type LIMS used in the multi-physics model. (a) and (b) show the same information except for arrangements of magnetic poles close to the drum surface. (a) Concurrent magnetic poles (CMP); (b) Alternating magnetic poles (AMP)

### 3.2. Modeling of magnetic field by the permanent magnet

In LIMS, the magnetic field generated by the permanent magnet (Nd-Fe-B, N48 grade) is a magneto-state problem because no electric current generates the magnetic field. Hence, formulating the problem using a magnetic scalar potential ($V_m$) is possible.

$$\boldsymbol{H} = -\nabla V_m, \tag{4}$$

$$\nabla\times\boldsymbol{H} = 0, \tag{5}$$

where **H** is the magnetic field. Using the constitutive relation between the remnant flux density of the permanent magnet (**Br**) and the magnetic field in Eq. (6):

$$\boldsymbol{B} = \mu_0\mu_m\boldsymbol{H} + \boldsymbol{Br}, \tag{6}$$

where $\mu_0$ is the magnetic permeability of vacuum, $\mu_m$ is the relative permeability of the permanent magnet. Then according to the equation: $\nabla\cdot\mathbf{B} = 0$. We can derive the Eq. (7):

$$\nabla\cdot(\mu_0\mu_m\nabla V_m + \boldsymbol{Br}) = 0. \tag{7}$$

### 3.3. Modeling of the particle properties

The slurry that flows across the tank comprises the MTMPs and water. To make this study more realistic and relevant today, the MTMPs are assumed to be spherical particles of radii $r_{mix}$ and contain three type of particles, namely, pure magnetite, pure quartz, and under-liberated interlocked quartz-magnetite particle, which has a certain volume percentage of magnetite and quartz. The density of the MTMP ($\rho_{mix}$) is related to the volume percentage of the magnetite ($\omega_m$) according to:

$$\rho_{mix} = 10^{-2}\omega_m(\rho_m - \rho_q) + \rho_q, \tag{8}$$

where $\rho_m$ and $\rho_q$ are the densities of pure magnetite and pure quartz, respectively. Furthermore, the relative permeability of the MTMP ($\mu_{r,mix}$) is assumed to be evenly distributed and is expressed by Eq. (9):

$$\mu_{r,mix} = 10^{-4}\omega_m^2(\mu_{r,m} - 1) + 1, \tag{9}$$

where $\mu_{r,m}$ is the relative permeability of the magnetite.

### 3.4. Modeling of the MTMPs tracing in multi-physics

Only three types of forces, namely, magnetophoretic, hydrodynamic, and centrifugal forces, are considered. The gravitational force is neglected because the size of MTMP lies in 0.074 mm. Particle to particle interactions, such as electrostatic, Van der Waals, and magnetic dipole-dipole are also neglected because of their inherent complexity. The magnetophoretic force that acts on a spherical magnetic particle of radius subjected to the magnetic field can be calculated by Eq. (10).

$$\boldsymbol{F}_m = 2\pi r_{mix}^3 \mu_0 \mu_r K \nabla \boldsymbol{H}^2, \tag{10}$$

where $\mu_r$ is the relative permeability of water. $K$ is the Clausius-Mossoti factor that uses magnetic permeability, which could be expressed by Eq. (11).

$$K = \frac{\mu_{r,mix} - \mu_r}{\mu_{r,mix} + 2\mu_r}. \tag{11}$$

Numerical analysis is performed to calculate the flow field and the behaviors of the MTMPs with consideration for hydrodynamic drag force ($\mathbf{F_D}$), as stated in the following equation:

$$\boldsymbol{F}_D = \frac{18\mu_w}{\rho_{mix} d_{mix}^2} m_{mix} (\vec{\boldsymbol{u}} - \overrightarrow{\boldsymbol{v}_{mix}}), \tag{12}$$

where $\mu_w$ is dynamic viscosity of water, and $m_{mix}$ is the mass of MTMP.

MTMPs are also subjected to centrifugal forces caused by rotating drum when MTMPs are frozen onto the drum surface. The centrifugal force is implemented for the drum surface as a constant for simplicity. It is calculated from linear velocity ($\mathbf{u}_l$).

$$\boldsymbol{F_c} = m_{mix} \frac{\boldsymbol{u_l}^2}{r_d}, \tag{13}$$

where $r_d$ is the radius of the drum.

### 3.5. Boundary conditions

Selecting appropriate inlet conditions for the Navier-Stokes equations is a non-trivial task. Specifying the velocity of the vector at the inlet and the outlet may cause convergence difficulties. Generally, the slurry enters the tank along the normal direction of the inlet boundary and moves out from the outlet boundary. Thus, velocity is specified at the inlet, whereas pressure is specified at the outlet. The normal inflow velocity is specified as

$$\boldsymbol{u} = -u_0 \boldsymbol{n}, \tag{14}$$

where $\mathbf{n}$ is the inlet boundary normal vector, and $u_0$ is the normal inflow speed. Pressure condition specifies the normal stress, which in most cases is approximately equal to pressure. The tangential stress component is set to zero. The reference pressure ($p_{ref}$), defined at the physics outlet level, is equal to 0, and the value of pressure ($p_o$) at the outlet boundary is the absolute pressure.

$$[-p\boldsymbol{I} + \mu(\nabla \boldsymbol{u} + (\nabla \boldsymbol{u})^T)]\boldsymbol{n} = -\hat{p}_0 \boldsymbol{n}, \tag{15}$$

$$\hat{p}_0 \leq p_0. \tag{16}$$

In particular, the suppress backflow check box is selected by default and is used to adjust the outlet pressure to prevent flurry from entering the tank through the outlet boundary.

The drum surface boundary condition is set as slip velocity to describe the rotary movement of the drum. The surface is sliding in its tangential direction. The drum does not have to actually move in the coordinate system. The linear velocity is given as a scalar $u_l$ and the condition prescribes

$$\boldsymbol{u}_{drum} = u_l \boldsymbol{t}, \tag{17}$$

where $\mathbf{u}_{\mathrm{drum}}$ is the tangential velocity, $\mathbf{t}$ is the drum surface boundary tangential vector.

In addition, the tank wall boundary condition is used to determine what happens to the MTMPs when they contact with the tank wall or when the drum surface is constructed. The specified tangential and normal velocities of the reflected particle velocity ($\mathbf{v}_\mathrm{p}$) are set up in the tangent-normal coordinate system ($\mathbf{t}_1$, $\mathbf{n}$). Resolution and convergence problems are solved by considering the energy loss in elastic collision:

$$\boldsymbol{v}_p = \begin{cases} cos\,\varphi \sqrt{2e\boldsymbol{v}_0}\,(\boldsymbol{t}_1) \\ sin\,\varphi \sqrt{2e\boldsymbol{v}_0}\,(\boldsymbol{n}) \end{cases}, \tag{18}$$

where $e$ is the energy loss rate, $\mathbf{v}_0$ is the velocity of the MTMP before it collides with the wall, and $\varphi$ is the angle of MTMP collides with the wall.

## 4. Results and discussion

In the time-dependent solver, the non-linear method of fully coupled model is specified as constant (Newton), where the damping factor is 0.9, the maximum number of iterations is 8, and the iterative error is less than 1%. The run time of a 50000-particle simulation using the model presented in this work corresponds to approximately 10 minutes on a 3.20 GHz, 64 bit, and 8 GB Ram Intel core i5-6500 processor. The other conditions and parameters are provided in Table 1.

Table 1. Conditions and parameters used in the multi-physics model

| Properties | Units | Values |
|---|---|---|
| Density of water（$\rho_w$） | Kg·m$^{-3}$ | 997.1 |
| Viscosity of water（$\mu_w$） | kg·m$^{-1}$s$^{-1}$ | 8.9×10$^{-4}$ |
| Average fluid flow velocity at the inlet（$\mathbf{u}_0$） | m·s$^{-1}$ | 1.0 |
| Volume percentage of magnetite in interlocked particle ($\omega_m$) | % | 30 |
| Multi-type magnetic particle (MTMP) of radius（$r_{mix}$） | mm | 7.4×10$^{-2}$ |
| Density of magnetite（$\rho_m$） | kg·m$^{-3}$ | 5050 |
| Density of quartz（$\rho_q$） | kg·m$^{-3}$ | 2800 |
| Remnant flux density of permanent magnet（**Br**） | T | 0.7 |
| Relative permeability of permanent magnet（$\mu_r$） | - | 1.33 |
| Relative permeability of magnetite（$\mu_{r,m}$） | - | 6.19 |
| Relative permeability of quartz（$\mu_{r,q}$） | - | 1 |
| Drum of radius（$r_d$） | mm | 300 |
| Energy loss rate（$e$） | - | 0.4 |
| Linear velocity of the drum（$\mathbf{u}_l$） | m·s$^{-1}$ | 0.1 |

### 4.1. Magnetic field intensity and gradient analysis results

Fig. 2 shows the magnetic field produced by AMP and CMP, respectively. The magnetic field intensity and gradient are highest at the corner of permanent magnet and abruptly weakened along the normal direction of the drum. The direction of the magnetic field gradient is represented by the red arrow in Fig. 2c, d. The arrow of the AMP always points to the permanent magnet assembly, but the magnetic field gradient generated by the CPM creates four repulsion zones near the drum surface.

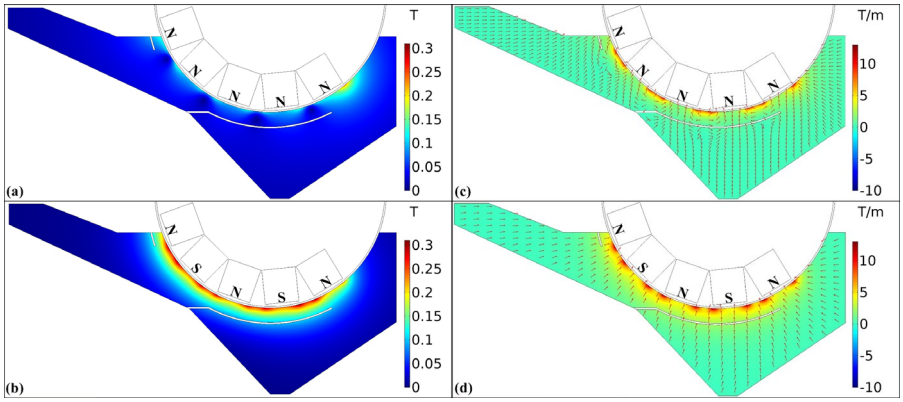


Fig. 2. The magnetic field and gradient are generated in the tank by CMP (a, c) and AMP (b, d). The color indicates the magnetic field intensity (a, b) and the magnetic field gradient (c, d). The red arrow indicates the direction of the magnetic field gradient

The average of magnetic field intensity and gradient at different distances from the drum surface are calculated, as shown in Fig. 3. The average magnetic field intensity of AMP at the drum surface and at 40 mm are 0.25 T and 0.09 T, respectively, which is twice that of CMP. In addition, the average magnetic

field gradient generated by AMP at the drum surface and at 40 mm is 7.10 T·m$^{-1}$ and 2.08 T·m$^{-1}$, respectively, which is 28.86% and 184% higher than that of CMP. The aforementioned results show that higher and more widely distributed magnetic field intensity and gradient are generated near the drum by AMP.

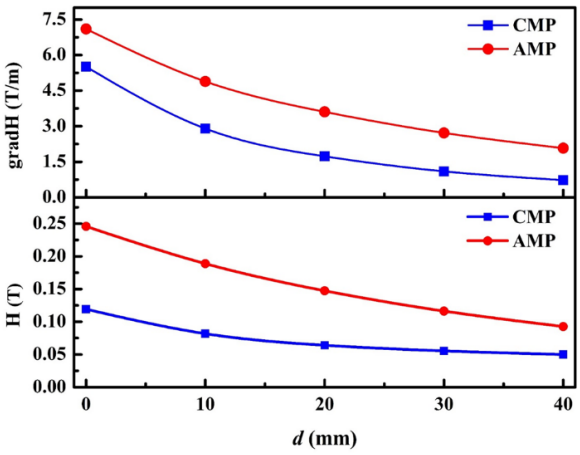


Fig. 3. Average magnetic field intensity and gradient calculated at five distances from the drum surface, where d= 0, 10, 20, 30, 40 mm

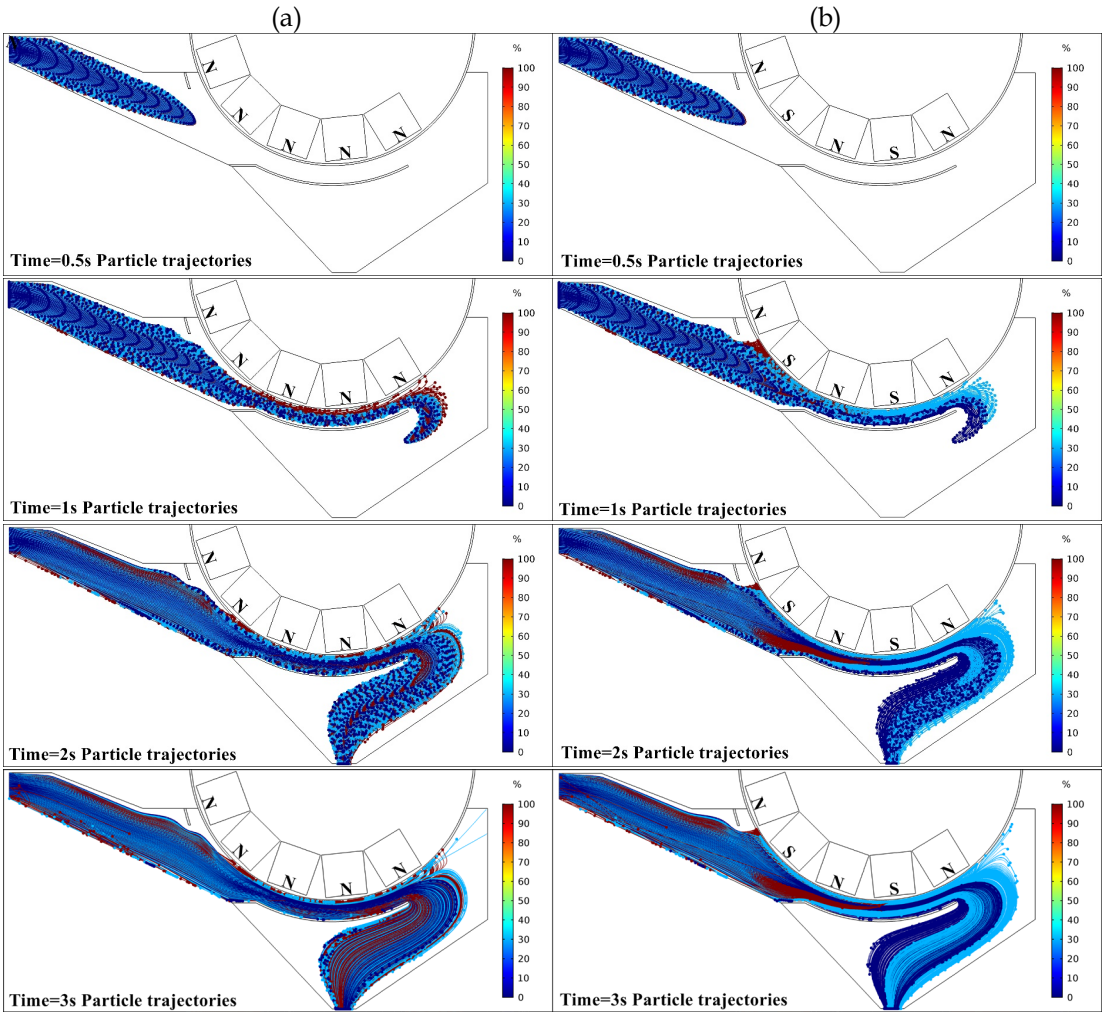


Fig. 4. 2D dynamic behavior of MTMPs in wet LIMS, where t = 0.5, 1, 2, 3 s. Particles are colored by the percentage magnetite content, and streamlines represent particle trajectories. (a) and (b) show the same information except for CMP and AMP

### 4.2. 2D Dynamic behavior of MTMPs in wet LIMS

Fig. 4b shows that the MTMPs enter the tank under the drag force, begin to separate under the influence of different magnetophoretic forces, and move toward the permanent magnet assembly. Among these particles, pure magnetite particles are first captured onto the drum surface. Interlocked particles are not captured until they move to the scavenger zone because they are subject to weak magnetophoretic force. However, non-magnetic minerals are not magnetically influenced and flow into the tailings along with the slurry under the influence of large fluid drag forces. Through this separation process, magnetic minerals and non-magnetic minerals are efficiently separated. It is worth noting that the MTMPs are subject to weaker magnetophoretic forces and are even excluded from the repellent zone, because of the lower magnetic field intensity and four repellent areas created by the CPM near the drum surface. Few of pure magnetite and interlocked particles are captured in the scavenger zone, and the remaining MTMPs flow out of the tailings outlet under the effect of fluid drag (see Fig. 2c and 4a).

Magnetite particle in LIMS always has a variable magnetization, depending on where it is situated relative to the drum. The particle can reach the saturation magnetization when the magnetic field intensity in which the particle is placed is high enough (above 0.6 T) (Murariu et al., 2013). By inspecting the color legend in Fig. 2, the permanent magnet assembly of the LIMS is shown to produces a much lower field, even very close to the drum surface (the highest is approximately 0.31 T at the drum surface in AMP). According to Equation (10), the magnetophoretic force on the MTMP is proportional to the magnetic field intensity under a non-uniform magnetic field. Therefore, if the particle is close to the drum, then the magnetic field intensity is higher. Consequently, magnetization is higher and the attractive magnetophoretic force is larger. If the distance to the magnet source is long, then the particle attracted to it might not be able to reach it before being carried away with the flow.

### 4.3. Effect of arrangements of permanent magnet assembly on recovery

The results in Fig. 5 show that the recovery of MTMPs increases with separation time. However, the total magnetic particle recovery of AMP is 69.90%, an increase of 51.75% over CMP. The recoveries of pure magnetite and interlocked particles in AMP are 93.51% and 48.75% and only 28.56% and 8.32% in CMP, respectively.

The results show that the different arrangements of the permanent magnet assembly will affect the dynamic behavior of the MTMPs and the separation efficiency. A high and widely distributed magnetic field intensity and gradient are generated near the drum by AMP. This arrangement causes the direction of the magnetic force that acts on the particles to always be toward the magnetic poles, and the magnetic particles are more easily adsorbed onto the drum surface. Hence, most magnetic particles can be captured from the flowing slurry selectively. This phenomenon also results in the use of AMP in the arrangement of permanent magnet assembly in the actual industrial production.

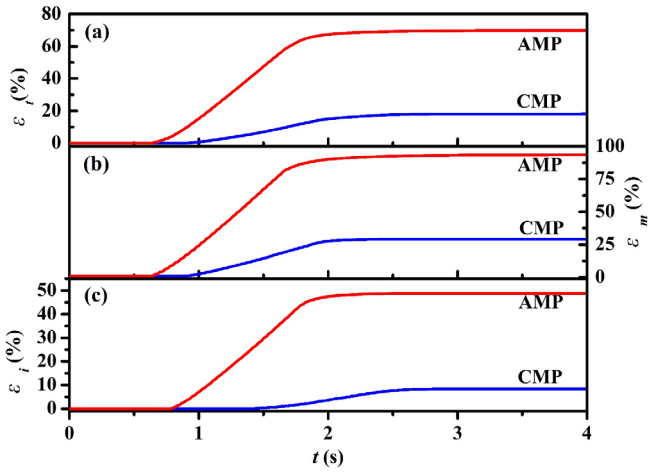


Fig. 5. Compares the recovery of MTMPs calculated as a function of capture time ($t$) for CMP and AMP. (a), (b), and (c) show the recoveries of total magnetic particles ($\varepsilon_t$%), pure magnetite ($\varepsilon_m$%) and interlocked particles ($\varepsilon_i$%), respectively

### 4.4. Effect of relative permeability of the interlocked particles on recovery

It can be seen from Fig. 6 that the relative permeability of the interlocked particle increases with increase in the volume percentage of the magnetite. According to equation (9), the relative permeability of interlocked particle is proportional to the square of volume percentage of magnetite. When the volume percentage of magnetite is 60%, the relative permeability of the interlocked particle is 2.98.

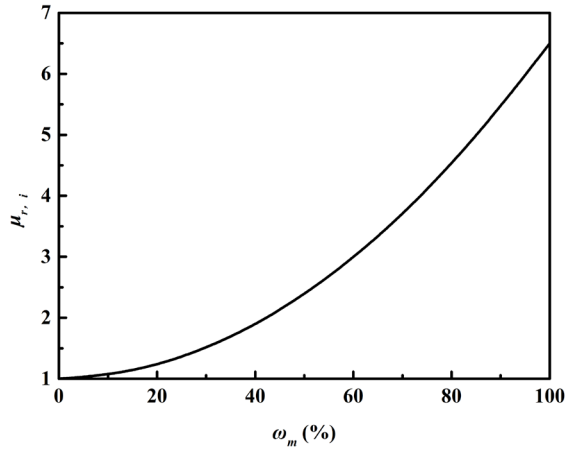


Fig. 6. The relationship between the relative permeability of interlocked particles and the volume percentage of magnetite

As shown in Fig. 7, when the relative permeability of interlocked particle is less than 2.98, the recovery of interlocked particles increases with a steep slope, but then the slope decreases dramatically. When the relative permeability in the contiguous granules is 2.98, the recovery of the contiguous granules has exceeded 90%. And according to equation (10), the magnetophoretic force on the interlocked particle is proportional to the relative permeability of the interlocked particle under a non-uniform magnetic field. This shows that the volume percentage of magnetite in the interlocked particles can easily affect the recovery and selectivity of the magnetite concentrate. The simulation results of the recovery rate are well verified by experiments.

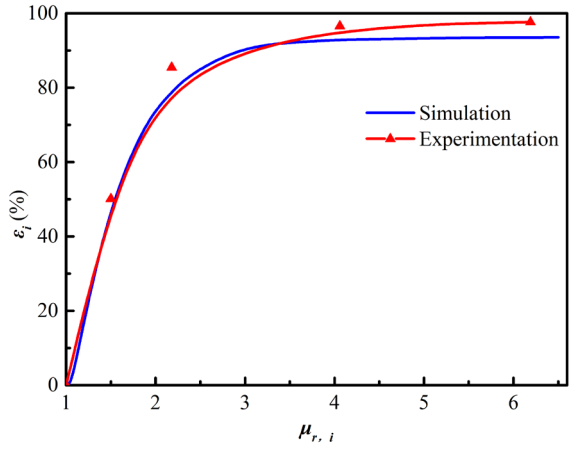


Fig .7. The relationship between the recovery rate of the contiguous particles and the relative magnetic permeability

### 4.5. Experimental verification of MTMPs accumulation

Validation is necessary to show shortcomings that are inevitable in model or simulation. $Fe_3O_4$ particles were collected from the Hongshan Mining Co., Ltd. (Yunnan, China). Only the size fraction of −100+60 μm is used in this work. The sample is assayed at 68.5% Fe and 5.1% $SiO_2$ with 5.19 magnetic susceptibility at room temperature. The simulated cumulative results of AMP are compared with the equilibrium shape of the particles in the LIMS of the laboratory.

Fig. 8 shows that magnetic particles are trapped and accumulated at the corners of the permanent magnet. Equation (10) shows that the level of the magnetophoretic force is dependent on the magnetic field gradient. The magnetophoretic force is generated intensively at the corner of the permanent magnet where the magnetic field intensity is concentrated. The distributions of magnetophoretic force affect the accumulation of MTMPs within the magnetic fields.

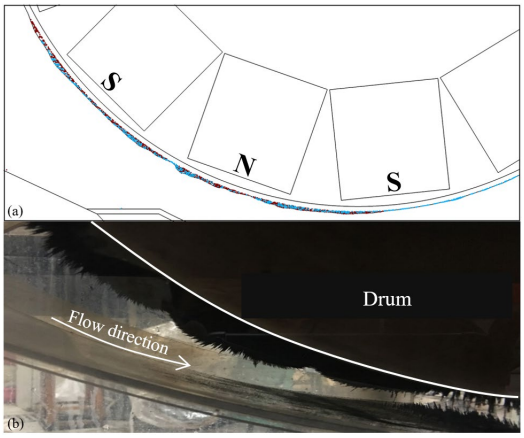


Fig. 8. The simulated cumulative result of AMP (a) is compared with the equilibrium shape of the magnetite in the LIMS of the laboratory (b)

## 5. Conclusions

A novel and straightforward, fully coupled multi-physics model was developed to investigate the 2D capture and accumulation of MTMPs in wet LIMS. All of the relationships were solved in COMSOL Multiphysics version 5.2a. The results from this model were analyzed in terms of the distribution of the magnetic field intensity and gradient, 2D dynamic behavior of MTMPs in LIMS, effect of arrangements of permanent magnet assembly on recovery and Effect of magnetic susceptibility of the interlocked particles on recovery. All of the aforementioned results show that the different arrangements of the permanent magnet assembly affect the distribution of magnetic field intensity and gradient in the tank; and the volume percentage of magnetite affects the relative permeability of the interlocked particle, thereby affecting the dynamic behavior of the MTMPs and the efficiency of separation. The results of accumulation from the model were also compared with the experiments and theory, and the correctness of the solutions obtained from COMSOL Multiphysics version 5.2a was demonstrated. The model described in this paper has been built for the wet CR configuration but can be easily adapted to any other configurations or even to dry magnetic separation or medium-intensity magnetic separator (MIMS). With further development, a fully coupled multi-physics model that concludes particle-fluid interaction coupling or magnetized particles that affect the magnetic field will be developed. Systematic comparison and study of various mechanisms and properties related to wet LIMS will be conducted. The effect of all geometric and operational parameters of the separator on efficiency or selectivity of mineral separation processes will be investigated. It can be used to predict performance changes as a function of operating/design parameters of the separator and improve the design of the wet LIMS.

## Acknowledgments

The authors gratefully acknowledge and appreciate the financial support provided by the National Natural Science Foundation of China (Grant No. 51764023).

## References

BIKBOV, M. A., KARMAZIN, V. V., BIKBOV, A. A. 2004, *Low-intensity magnetic separation: principal stages of a separator development – what is the next step?,* Physical Separation in Science Engineering, 13(2), 53-67.

CHOOMPHON-ANOMAKHUN, N., EBNER, A. D., NATENAPIT, M., RITTER, J. A. 2017, *Simulation of dynamic magnetic particle capture and accumulation around a ferromagnetic wire,* Journal of Magnetism Magnetic Materials, 428, 493-505.

DRIVER D. M., H. L. SEEGMILLER. 1985, *Features of a reattaching turbulent shear layer in divergent channel flow,* Aiaa Journal, 23(2), 163-171.

ERSAYIN, S. 2013, *Low intensity magnetic separator modelling: a pseudo liberation approach,* Mineral Processing Extractive Metallurgy, 113(3), 167-174.

GARCIA-MARTINEZ, H. A., SONG, S., LOPEZ-VALDIVIESO, A. 2011, *In situ observation of quartz particles entrained into magnetite coagulates in a uniform magnetic field,* Minerals Engineering, 24(8), 963-966.

KLEIV, R. A., & THORNHILL, M. 2011, *Dry magnetic separation of olivine sand.* Physicochemical Problems of Mineral Processing, 47(47), 213-228.

LEJON ISAKSSON, L. 2008, *Våta svagmagnetiska separatorer - modeller och funktion.* Master thesis, Luleå University of technology.

LINDNER, J., MENZEL, K., NIRSCHL, H., 2013. *Simulation of magnetic suspensions for HGMS using CFD, FEM and DEM modeling.* Comput. Chem. Eng. 54, 111–121.

MURARIU, V. 2013, *Simulating a Low Intensity Magnetic Separator Model (LIMS) using DEM, CFD and FEM Magnetic Design Software,* In: Proceedings of Computational Modelling'13, Falmouth, UK. Computational Modeling.

PRAKASH, S., DAS, B., MOHAPATRA, B. K., & VENUGOPAL, R. 2000, *Recovery of iron values from iron ore slimes by selective magnetic coating,* Separation Science & Technology, 35(16), 2651-2662.

RASOOL, R., & LIEBERWIRTH, H. (2018). *A continuum based numerical modelling approach for the simulation of whims.* Minerals Engineering,118, 97-105.

RAVNIK, J., HRIBERŠEK, M., 2013. *High gradient magnetic particle separation in viscous flows by 3D BEM. Comput.* Mech. 51 (4), 465–474

RAYNER, J. G. *The development of process models of the wet drum magnetic separator /,* Mathematical Model. 1999.

RAYNER, J. G., NAPIER-MUNN, T. J. 2000, *The mechanism of magnetics capture in the wet drum magnetic separator,* Minerals Engineering, 13(3), 277-285.

RAYNER, J. G., NAPIER-MUNN, T. J. 2003, *A mathematical model of concentrate solids content for the wet drum magnetic separator,* International Journal of Mineral Processing, 70(1), 53-65.

RAYNER, J. G., NAPIER-MUNN, T. J. 2003, *A mathematical model of recovery of dense medium magnetics in the wet drum magnetic separator,* International Journal of Mineral Processing, 69(1-4), 157-173.

SINGH, V., NAG, S., TRIPATHY, S. K. 2013, *Particle flow modeling of dry induced roll magnetic separator,* Powder Technology, 244(4), 85-92.

STENER, J. F., CARLSON, J. E., PÅLSSON, B. I., SAND, A. 2014, *Evaluation of the applicability of ultrasonic velocity profiling in conditions related to wet low intensity magnetic separation,* Minerals Engineering, 62, 2-8.

STENER, J. F., CARLSON, J. E., SAND, A., PÅLSSON, B. I. 2016, *Internal flow measurements in pilot scale wet low-intensity magnetic separation,* International Journal of Mineral Processing, 155, 55-63.

SUNDBERG, R.T., 1998. *Wet low intensity magnetic separation of iron ore.* In: Atak, S., Önal, G., Celik, M.S. (Eds.), Innovations in Mineral and Coal Processing, 7th ed. A.A. Balkema, Rotterdam, Netherlands, pp. 711–715.

TRIPATHY, S. K., BANERJEE, P. K., SURESH, N., MURTHY, Y. R., & SINGH, V. 2017. *Dry high-intensity magnetic separation in mineral industry – a review of present status and future prospects.* Mineral Processing & Extractive Metallurgy Review, *38*(4), 339-365.

WILCOX, D. C. *Turbulence modeling for CFD.* Turbulence modeling for CFD /, DCW Industries. 2006.